



Repositorio Institucional de la Universidad Autónoma de Madrid

<https://repositorio.uam.es>

Esta es la **versión de autor** del artículo publicado en:

This is an **author produced version** of a paper published in:

Energy and Fuels 30.11 (2016): 9510-9516

DOI: <http://dx.doi.org/10.1021/acs.energyfuels.6b02112>

Copyright: © 2016 American Chemical Society

El acceso a la versión del editor puede requerir la suscripción del recurso

Access to the published version may require subscription

Biomass-derived microporous carbon materials with open structure of cross-linked submicrofibers with enhanced adsorption characteristics

*Francisco Heras^{*1}, Diana Jimenez-Cordero¹, Miguel A. Gilarranz¹, Tarik R. Smith²,
Noelia Alonso-Morales¹, Juan J. Rodriguez¹*

¹ S.D. Ingeniería Química. Universidad Autónoma de Madrid. Ctra. Colmenar Viejo,
km 15. 28049 Madrid (Spain)

² Koom Consulting. C/ Topete, 15. 08221. Tarrasa (Spain).

Abstract

Moringa oleifera seed shells exhibit a unique structure of cross-linked submicrofibers (0.5 – 1.5 μm diameter) with a well-connected macroporous network. Controlled pyrolysis (500-800°C) and cyclic activation of precursor provided a porous carbon material with a structure that minimizes mass transfer constraints. Under both slow (10°C/min⁻¹) and flash pyrolysis the structure was preserved, while a significant microporosity was developed. By flash pyrolysis (700-800°C), a material with enhanced characteristics for potential application as molecular sieve ($S_{\text{DA}}=450\text{-}470\text{ m}^2\text{g}^{-1}$; $S_{\text{BET}}=$

*Corresponding autor. Ph.: +34914978051. Fax: +34914973516. E-mail: fran.heras@uam.es

5 m²g⁻¹) was obtained. Cyclic activation of carbonized shells, consisting in an oxygen chemisorption stage (180°C) followed by a desorption stage in inert atmosphere (450-900°C), resulted in a controlled development of microporosity upon successive activation cycles. After ten activation cycles, respective S_{DA} and S_{BET} values of 1172 and 761 m²g⁻¹ were obtained. Higher development of surface area and a wider distribution of micropores was observed when desorption stage was carried out at 900°C. The development of surface area was achieved at low burn-off (22-33%), thus preserving the structure of the material. Thanks to its unique structure the material obtained exhibited enhanced characteristics for gas sorption due to diminished mass-transfer limitations, assessed through the kinetics of carbon dioxide adsorption runs at ambient conditions.

Keywords: biomass, activated carbon, adsorption, carbon microfibres

1. Introduction

Agricultural biomass by-products and wastes are potential precursors for a large variety of materials and entail a broad range of applications; bioadsorbents, composites and porous carbons, being among the most commonly reported¹⁻⁶. The valorization of biomass by-products and wastes can be an important contribution to local economies, particularly in developing areas, with locally available plant species playing a key role. *Moringa oleifera* is the most widespread species of the plant family Moringaceae. It is a tree that is both cultivated and naturally found and can grow in zones with both humid and hot dry climate including Northern India, Africa and the Caribbean⁷. It is considered as a “multipurpose tree”, thus in addition to wood the dried seeds can be used to produce a high quality vegetable oil with a number of applications including

medical uses^{8,9}. In the recent years, special attention has also been paid to the natural coagulants obtained from moringa seeds, which can be used in water treatment processes¹⁰. Extracted seeds, pods and husk resulting from processing are commonly used as fuels, although the use for the preparation of porous carbons from husks has also been studied.

Pollard et al.¹¹ and Warhust et al.¹² reported on the use of moringa husks for the preparation of microporous activated carbon by way of pyrolysis, steam pyrolysis and steam activation. Although the overall yield of the process was low, the resulting microporous material also showed an ordered macropore network derived from the structural characteristics of the starting husks. This structure confers reduced mass-transfer constraints, as evidenced by a remarkably high rate of phenol and nitrophenol adsorption in liquid phase¹².

The production of carbonaceous porous materials from lignocellulosic agricultural wastes or by-products has been an established and productive field within carbon research for many years¹³⁻¹⁶. It has been shown that the morphology and macropore structure of the precursor plays a key role in the performance of the resulting material, enhancing mass transfer and handling^{19,18}. However, preparation methods that minimize burn-off and preserve the tissue structure are needed to take advantage of the starting morphology and structure.

Cyclic activation by oxygen chemisorption-desorption has been proposed as an interesting solution for a controlled activation that enables tailoring of carbon materials through targeted porosity development^{16,19,20}. That way consists of a chemisorption step at relatively low temperature followed by desorption in an inert atmosphere at high temperature. The sequence is repeated until the intended development of porosity is

achieved. This method can provide an efficient way to create whole porosity from a precursor and to controllably modify the porous structure of a carbonaceous material.

Previous works on the cyclic activation of grape seed char¹⁶ and waste tyres char²⁰ with air showed that the development of surface area takes place at burn-off values below or within the lowest range reported for the physical activation of these starting materials. This controlled burn-off was also shown to be crucial for maintaining the initial morphology of the char upon activation.

The objective of this investigation is to study the preparation of carbon porous materials by pyrolysis and cyclic activation with air of *Moringa oleifera* seed husk, with a focus on both the preservation of the starting material structure and the controlled development of porosity. To assess the low mass transfer constraints conferred to the material by the structure of sub-microfibers, preliminary carbon dioxide adsorption tests were carried out.

2. Material and Methods

The starting material used in this study was seed husk from *Moringa oleifera* cultivated in Burkina Faso. The husk was separated from the seed, washed with distilled water repeatedly until no turbidity was observed, dried at 105°C for 1 day, milled to reach a size between 0.5 and 2mm and stored refrigerated until use.

2.1. *Samples characterization*

Prior to pyrolysis runs, the starting material was characterized by TGA with a Mettler SDTA851e apparatus. The gas flow (N_2 or air) was 100 mLmin^{-1} (all flows referred to normal conditions) and the heating rate was $10^\circ\text{C min}^{-1}$. The weight change of a sample with temperature and/or time in a controlled atmosphere during TGA runs provides information about decomposition, oxidation or dehydration processes driven from thermal treatment. This technique allowed also establishing the temperature ranges for the oxidation and desorption steps of the activation cycles. To study oxygen chemisorption at isothermal conditions, the samples were heated in nitrogen atmosphere until the programmed temperature was reached, then the gas flow was switched from nitrogen to air.

The elemental analysis (C, N, H and S) of the samples was performed with a LECO CHNS-932 apparatus. The ash mass fraction was determined by calcination in air at 800°C for 2 h. Surface area and total pore volume of the samples were measured in an automated volumetric gas adsorption Micromeritics apparatus (Tristar 3020) by adsorption of N_2 at 77 K, and CO_2 at 273 K. Approximately 0.15 g of sample were used in each test. The weighed samples were placed in a glass container and degassed at 150°C during 7 h under vacuum (10^{-3} Torr) prior to adsorption measurements using a Micromeritics sample degas system (VacPrep 061). The N_2 adsorption-desorption isotherms were obtained within the $10^{-5} - 1.0 \text{ P/P}_0$ range, although the P/P_0 range used to calculate the BET surface area (S_{BET}) was $0.05 - 0.3^{21}$. The t-method was used for the micropore volume (V_{microN_2}) and BJH for obtaining the narrow-mesopore volume ($V_{\text{Narrow-meso}}$), total mesopore volume ($V_{\text{mesoTOTAL}}$) and mean mesopore width ($\text{dpore}_{\text{N}_2}$)²². Dubinin-Astakhov (DA) model was applied to the CO_2 isotherms to determine the DA surface area (S_{DA}), micropore volume (V_{microCO_2}) and mean micropore

width ($\Delta p_{\text{poreCO}_2}$)²³. The Non-Local Density Functional Theory (NLDFT) with pore geometry slit was used to calculate the pore size distribution from both the CO₂ and N₂ isotherms²⁴. The applicability of this procedures for biomass chars and chars activated by cyclic activation with air was discussed in a previous work¹⁶.

The morphology of the moringa seed husk-derived samples was analyzed by scanning electron microscopy (SEM) performed with a Hitachi S-3000N apparatus. The specimens for SEM observation were metalized with gold to prevent electrical charging during examination using a sputter coater SC502. Imaging was done in the high vacuum mode under an accelerating voltage of 20kV, using secondary electrons.

2.2 Pyrolysis

The pyrolysis of samples was carried out in a vertical quartz tube (68 cm length and 4.8 cm i.d.) placed in a sandwich-type electrical furnace. A 100 mLmin⁻¹ nitrogen flow was continuously passed downward. Two K-type thermocouples placed on the furnace wall and the central part of the reactor were used to control the temperature. The operating variables tested were: heating rate (SH: slow heating at 10°C min⁻¹ ; FH: flash heating) and set temperature (300 – 1000°C). Flash pyrolysis has been defined as a process characterized by rapid devolatilization in an inert atmosphere at high heating rate and reaction temperatures between 450 and 1000°C. For the SH samples, a quartz basket with 4-5 g of moringa seed husk was placed in the central part of the reactor, air was purged and then heating of the system was started. For the preparation of FH samples, the basket was kept in the top cold zone of the tube in order to heat the central zone to the desired temperature and remove any air present, and then displaced to the central hot

zone by means of a rod. After the pyrolysis, the basket was cooled in the cold zone and finally the char was recovered²⁵.

The carbonized samples obtained were labeled by the pyrolysis temperature followed by the heating rate, e.g. for the sample 600FH, pyrolysis was carried out at 600°C using flash heating.

2.3 Cyclic activation

The activation of all the samples was carried out in a vertical quartz tube (70 cm length and 3.5 cm width) placed in an sandwich-type electrical furnace under controlled heating rate, temperature and gas flow. The oxidation step of each cycle was performed at 180°C for 2h under a 100mL min⁻¹ air flow. The desorption stage was carried out at two different temperatures (450 and 900°C) using a nitrogen flow rate of 100mLmin⁻¹ and 2h at the final temperature. The switch from chemisorption to desorption temperature was carried out at a heating rate of 10°Cmin⁻¹ under nitrogen flow. The activated samples were designated by the oxidation temperature, desorption temperature and the number of cycles used, e.g. for sample 180-450 C2 oxidation was carried out at 180°C, desorption at 450°C and two oxidation-desorption cycles were completed. After each activation cycle, the reactor was cooled under nitrogen flow and the activated sample was collected to estimate the burn-off and perform the textural characterization. Burn-off values were calculated as the weight-loss respect to the initial char in a dry basis (d.b.).

2.4. Carbon dioxide adsorption runs

Two selected samples of moringa seed husk char showing different pore structure were tested in carbon dioxide adsorption. To check the positive influence of the morphology of moringa seed husk char on the kinetics of adsorption, a char with similar pore structure obtained by pyrolysis of grape seeds was used as a reference²⁶. The samples were grinded to a size between 1 and 2 mm. The carbon dioxide adsorption runs were carried out in a Mettler-Toledo thermobalance. Before the thermogravimetric analysis (TGA), the samples were vacuum de-gasified at 120°C during 8h. The tests were carried out at a constant temperature of 35°C. Firstly, the sample was stabilized during 90min under nitrogen flow and then the gas flow was switched to pure carbon dioxide (100NmLmin⁻¹).

3. Results and Discussion

3.1. Pyrolysis

The SEM images of the crushed *Moringa oleifera* seed husk shown in Fig. 1 indicate that this material has a unique structure composed of crosslinked fibers with diameters below 2 μm . The open structure of the material, with a relatively ordered network of well-connected macropores can be of great interest for its use as biadsorbent, since mass transfer limitations within the material matrix would be minimized. The protective function of the seed husk can provide additional strength compared to other materials, as it has been shown for other seed-based carbon materials¹⁶⁻²⁶.

Figure 1. Selected SEM images of crushed *Moringa oleifera* seed husk.

Fig. 2 shows the TGA curves for the starting moringa seed husk in N₂ atmosphere and final temperatures between 300 and 900°C. The initial peak is ascribed to the loss of water, which amounts for 7-8% of the initial sample weight. The curves show that the bulk weight loss ascribable to pyrolysis occurs between 300 and 500°C. At temperatures below 500°C, important differences observed about pyrolysis yield in char were observed (from 50 to 35 %, approx.), whereas only a slight additional weight loss is observed above 800°C. These results indicate that the pyrolysis process is incomplete within 300-500°C range. The pyrolysis yield values at temperatures higher than 500°C are 25-30%. In addition, pyrolysis temperatures above 800°C have been reported to lead to the collapse of the microporous structure for other biomass materials¹³. Therefore, according to these results a pyrolysis time of 2 h and the temperature range between 500 and 800°C were selected for a deeper study of the pyrolysis of moringa seed husk.

Figure 2. TGA of Moringa seed husk in N₂ atmosphere at different final temperatures (10°C min⁻¹ heating rate).

The elemental composition of the carbonized samples obtained at different conditions (Table 1) shows an increase in the carbon content as the pyrolysis temperature increases from 500 to 800°C. Simultaneously, a reduction of hydrogen content takes place, evidencing the loss of hydrogen containing volatile matter. The ash content of the precursor is relatively high, about 12% of precursor samples that means about 21% of pyrolyzed samples. The chars obtained can be considered as virtually sulfur-free.

Table 1. Composition (% w, d.b.) of the carbonized materials obtained under different pyrolysis conditions.

The starting material has a negligible surface area that increases dramatically upon pyrolysis due to the loss of volatile matter. The results in Table 2 show that the S_{DA} value, i.e. the surface area corresponding to the narrow micropores, increased substantially as the temperature was increased from 500 to 600°C at both conventional (low heating rate) and flash pyrolysis. Further heating at higher temperature only results in slight increase of S_{DA} values. A remarkable surface area value of around 470 m²g⁻¹ was obtained, with no differences between FH and SH pyrolysis. It is relevant to point out that increasing pyrolysis temperature led to radical changes of the pore size distribution. Thus, up to a pyrolysis temperature of 600°C the S_{BET} values also increase, showing that both, narrow and wide micropores, contribute to the porosity of the material (mesoporosity is negligible in all cases). At 700-800°C the contribution of wider micropores decreases dramatically, this effect being much more pronounced in the case of the FH pyrolysis. The substantial difference between S_{DA} (450-470 m²g⁻¹) and S_{BET} (\approx 5 m²g⁻¹) indicates that the material can have potential application as a molecular sieve.

Table 2. Surface area (m²g⁻¹) and pore volume (cm³g⁻¹) of the carbonized materials obtained by pyrolysis.

3.2 Porosity development by cyclic activation

The carbonized material obtained by SH pyrolysis at 600°C was subjected to cyclic activation. The selection of this material was based on its high S_{DA} and also quite significant S_{BET} , indicating a much wider pore size distribution than the chars obtained at lower and higher pyrolysis temperatures. This structure is of interest to avoid diffusion constraints during oxygen chemisorption, such as the blockage of pores due to the allocation of surface oxygen groups at pore mouths²⁹.

Prior to the activation study, isothermal TGA tests of oxygen chemisorption by the char were carried out in air between 180 and 240°C (Fig. 3a). Although chemisorption is expected to occur within the range of temperature studied, some simultaneous desorption of uptaken oxygen can take place¹⁶; this seems more evident in the 240°C chemisorption test. The substantial difference between this weight-loss curve and the obtained at lower temperature denotes the occurrence of uncontrolled burn-off at that highest temperature. The lowest weight loss at 180°C indicates a higher contribution of oxygen chemisorption respect to burn-off reactions. Figure 3b shows the non-isothermal TGA tests in nitrogen atmosphere (desorption step) for the chars previously subjected to chemisorption. The highest loss of weight during this desorption step was observed for the char oxidized at 180°C, indicating a higher amount of oxygen chemisorbed and better conditions for generating burn-off and porosity due to the more labile groups generated at that temperature, which was therefore selected in the following for the chemisorption stage of the cyclic activation experiments. Figure 3b also shows a gradual loss of weight, with shoulders at around 300 and 600°C. From these data, two temperature values, 450 and 900°C, were selected for the desorption stage of the activation cycles to check the potential effect of the desorption of surface oxygen

groups of different nature in the generation of porosity. Both for the chemisorption and desorption stage a holding time of 2h at the respective final temperature was chosen.

Figure 3. TGA experiments (a) isothermal chemisorption tests in air for carbonized material, (b) non-isothermal desorption tests in nitrogen for carbonized material subjected to chemisorption at different temperatures.

Regarding the activation experiments, under all the combinations of oxidation and desorption temperatures tested, the burn-off increased almost linearly with the number of activation cycles (Figure 4). As a general trend, the highest burn-off was observed in the series of samples subjected to a desorption temperature of 900°C (Figure 4b), consistently with the highest desorption of chemisorbed oxygen observed at this temperature. The burn-off values achieved were still fairly low after 10 activation cycles at the two desorption temperatures tested (22 and 33 % at 450 and 900 °C, respectively).

Figure 4. Burn-off versus number of activation cycles at different activation conditions.

The development of surface area with the number of cycles performed is depicted in Figure 5. An important increase of S_{DA} was observed from the first cycle for the 180-900 series, reaching a remarkable value of $1270 \text{ m}^2\text{g}^{-1}$ after ten cycles. The generation of S_{DA} increase significantly from the 5-6th cycle. On the contrary, when the desorption stage was carried out at 450°C a substantially lower development of surface area took

place. Thus, the surface oxygen groups desorbed above 450°C must be important in the development of S_{DA} , those groups being mainly ascribed to phenols, carbonyl, quinones, lactones and in some extent carboxylic anhydride^{30,31}. A quasi-linear dependence with the number of cycles applied can be observed.

The S_{BET} decrease in the first activation cycle and then increase steadily, reaching around 670 m²g⁻¹ in the 180-900 series. The higher development of surface area for this series is consistent with the higher burn-off values achieved (see Figure 4). The differences in the S_{BET} achieved at the two activation conditions tested are not as important as in the case of S_{DA} . The significantly higher values of this last are indicative of a predominantly narrow microporosity of the resulting activated carbons.

Figure 5. Specific surface area (BET and DA) versus number of activation cycles under the two different conditions tested.

Warhurst et al.¹² obtained activated carbons by steam pyrolysis of *Moringa oleifera* husks at temperatures between 700-800°C. Activation at 700-750°C resulted in surface areas of 549-637 m²/g and overall yields of 15-17%. An increase of activation temperature up to 800°C led to a surface area of 774-932 m²/g at the expense of lower overall yield (9%). Pollard et al.¹¹ reported on the activation of *Moringa oleifera* husks char with steam at 850°C, obtaining a surface area of 734 m²/g and an overall yield of 10% (65% burn-off). Therefore, the current work shows that activated carbons with well-developed porosity can be obtained from *Moringa oleifera* husks with overall yields higher than from other physical activation methods. This feature of cyclic

activation has also been shown for the activation of grape seed¹⁶ and waste tire char²⁰, which is of great interest to preserve the morphology and mechanical strength.

Figure 6 shows the development of surface area per unit of burn-off along the 10-cycle test. Even though the S_{BET} of the samples increases with the number of activation cycles, thus providing a larger surface area available for chemisorption, no important differences are observed between the two activation series. However, the burn-off is slightly more selective towards the generation of surface area at a desorption temperature of 450°C.

Figure 6. Variation of S_{BET} /burn-off versus number of cycles at different activation conditions.

As it can be inferred from the S_{DA} and S_{BET} values obtained upon activation, the materials obtained are essentially microporous. The mesopore volume was almost negligible, representing those within the 2 – 8 nm range less than one-third of the total mesopore range. The evolution of the micropore volume with the number of cycles (Figure 7) is consistent with the pattern of the surface area development. The mean size of the narrow micropores, i.e. those measured by CO_2 adsorption, increase with the number of cycles, indicating that in addition to the creation of micropores, some widening of the existing ones is taking place. This can also be seen from the decrease of the mean size of the micropores measured by N_2 adsorption, as the widening of the narrow micropores makes them accessible to N_2 . On the other hand, no significant development of mesoporosity (both narrow and total mesoporosity) was observed with

the activation cycles applied, keeping the successive activated carbons the initial values of mesoporosity (around 0.02 – 0.03 and 0.005 – 0.010 cm³/g of narrow and total mesoporosity, respectively) showed by the chars.

Figure 7. Micropore volume development from N₂ isotherms along the cycles at the two different activation conditions.

The pore size distribution (PSD) is a key issue of the characterization of activated carbons and a number of methods have been developed for that purpose. The non-local density functional theory (NLDFT) has been widely used for the characterization of the pore structure of activated carbons and other porous materials²⁴. As can be observed in Figure 8, all the carbons obtained are clearly microporous with important contribution of narrow-micropores and ultramicropores. The microporosity pattern is quite similar for all the samples, with a homogeneous distribution characterized by three important contributions centered at 0.47, 0.55 and 0.87 nm in all cases, even for the char. Regarding mesoporosity, it has a low contribution, with some noticeable increase for the samples obtained after 10 activation cycles in the 2-4 and 10-50 nm ranges, this last mostly deriving from the starting char.

Figure 8. Pore size distribution as obtained by NLDFT method from CO₂ (a) and N₂ (b) isotherms for selected samples: char and activated carbons upon ten cycles at the two different conditions tested.

Figures 9, 10 and 11 show the SEM images of the pyrolysed seeds husk and activated carbons obtained after 5 and 10 activation cycles at desorption temperatures of 450 and 900°C. The morphology and macropore structure of the precursor was well preserved in the pyrolysis step, although some rearrangement of the crosslinked microfibers can be appreciated. Both the precursor and the char show a well-defined structure of cross-linked fibres and lamellae derived from the starting material. Activation seems to lead to a less regular pattern. The fibres show diameters between 0.5 and 1 μm but most of them are in the submicro scale, within 0.5 and 0.7 μm .

Therefore, the carbonization and activation of the precursor by the method investigated maintain the original open structure of crosslinked fibers, which is of great interest. The carbonization step promotes the hydrophobic character of the surface, useful for the adsorption of non-polar species. On the other hand, the subsequent leads to a well-developed microporous structure, with low contribution of mesopores, that combined with the macroporosity can favor applications in gas-phase increasing mass-transfer kinetics. Pyrolysis itself has been found to lead to tunable narrow microporosity under the appropriate conditions²⁶.

Figure 9. Selected SEM micrographs of pyrolysed seeds husk (600SH sample).

Figure 10. SEM micrographs of activated samples subjected to desorption at 450°C (a) 180-450C5 and (b) 180-450C10.

Figure 11. SEM micrographs of activated samples subjected to desorption at 900°C (a) 180-900C5 and (b) 180-900C10.

3.3. Carbon dioxide adsorption tests

As shown above, the carbon materials prepared from moringa seed husk exhibit a unique structure that can be of great interest as it can contribute to diminished mass transfer constrains. To prove this concept, preliminary carbon dioxide kinetic runs were carried out. The samples selected for this study were the chars obtained by flash pyrolysis of moringa seed husk at 600 and 800 °C (600FH and 800FH, respectively). These two samples showed similar morphology but some differences in pore structure. For comparison purposes, a char obtained by flash pyrolysis at 800°C of grape seeds²⁶ was also considered in the study (GS800FH). In Table 3, the specific surface area from N₂ (S_{BET}) and CO₂ (S_{DA}) adsorption isotherms of the three selected char samples are shown, while Figure 12 shows a SEM image of MO800FH to illustrate the morphology and the PSD calculated from CO₂ adsorption-desorption isotherm, of this reference sample.

Table 3. Specific surface area of chars selected for carbon dioxide adsorption runs

Figure 12. SEM micrographs of grape seed char (GS800FH)

Figure 13 shows the carbon dioxide adsorption kinetic curves for the samples studied. As can be observed, both chars prepared from moringa seed husk show identical carbon dioxide adsorption kinetics behavior, reaching the saturation in 4 - 6 min after switching the gas atmosphere from nitrogen to carbon dioxide. Comparing the adsorption capacities exhibited to textural properties of the samples, it can be deduced that both microporosity and micropore-centered pore size distribution are the most influential characteristics on adsorption capacity: the 800FH char exhibits a much higher adsorption capacity being the sample with higher narrow microporosity (S_{DA}) and lower mesoporosity and wider microporosity (S_{BET}); even higher capacity than GS800 with similar S_{DA} .

But, as the most interesting aspect for the purpose of this work, moringa seed husk chars show similar adsorption and saturation rates, both extremely higher than grape seed char, evidencing that moringa seed husk char has a morphology that facilitates transport within the bulk granules. Interestingly, 600FH and 800FH show similar adsorption and saturation rates, even though 800FH has a narrower distribution of micropores, indicating that narrow micropores are easily accessible thanks to the low diameter of fibers 0.5-0.7 μm . Therefore, it is proved that porous carbons obtained from moringa seed husk are characterized by a morphology that facilitates applications where low mass transfer constrain is required

Figure 13. Carbon dioxide adsorption kinetic runs for chars prepared from moringa seed husk (MO600FH, MO800FH) and grape seeds (GS800FH).

4. Conclusions

Pyrolysis and activation of *Moringa oleifera* seed husk upon cycles of oxygen chemisorption followed by thermal desorption allowed obtaining porous carbon materials with a macropore structure composed of cross-fibers with sub-micronica diameter (0.5 – 1 μm). That structure derived from the precursor and was well preserved under all the conditions tested. In addition to this, the char and the activated carbons showed a microporous structure.

Flash pyrolysis of the starting material at 700-800°C resulted in fairly high S_{DA} values (450-470 m^2g^{-1}), with a frankly small S_{BET} , almost negligible (5 m^2g^{-1}). During cyclic activation of the carbonizate at 180°C oxygen chemisorption temperature, development of surface area at low burn-off took place. Subsequent desorption at 900°C allowed higher development of surface area. After ten activation cycles, S_{DA} and S_{BET} values of 1172 and 761 m^2g^{-1} were obtained. Some widening of pores was observed during activation, although the resulting activated carbons were essentially microporous with a high contribution of narrow micropores and almost negligible presence of mesopores.

Testing of the moringa seed husk char in the adsorption of carbon dioxide proved that the material is characterized by diminished mass transfer constrains thanks to its unique structure and low diameter of the cross-fibers, which provides with readily accessible narrow microporosity.

Acknowledgments

The authors greatly appreciate financial support from the Spanish Ministerio de Economía y Competitividad (CTQ2012-32821).

References

1. El-Sheikh, A.H.; Newman, A.P.; Al-Daffae, H.K.; Phull, S.; Cresswell, N., *J. Anal. Appl. Pyrol.* **2004**, *71*, 151-164.
2. M. Bilal, M.; Shah, J.A.; Ashfaq, T.; Mubashar, S.; Gardazi, H.; Tahir, A.A. et al. *J. Hazard. Mater.* **2013**, *263*, 322-33.
3. Hubbe, M.A.; Hasan, S.H.; Ducoste, J.J. *Bioresources*, **2011**, *6*(2), 2161-2287.
4. Mohanty, A.K.; Misra, M.; Drzal, L.T.; *J. Polym. Environ.* **2002**, *10*(1-2), 19-26.
5. Titirici, M.M.; Antonietti, M. *Chem Soc Rev* **2010**, *39*(1), 103-116.
6. Savova, D.; Apak, E.; Ekin, E.; Yardim, F.; Petrov, N.; Budinova, T. et al. *Biomass Bioenerg.* **2001**, *21*(2), 133-142.
7. Nadeem, M.; Mahmood, A.; Shahid, S.A.; Shah, S.S.; Khalid, A.M.; McKay, G. J. *Hazard. Mater. B* **2006**, *138*, 604-613.
8. Warhurst, A.A.M.; Fowler, G.D.; McConnachie, G.L.; Pollard, S.J.T. *Carbon* **1997**, *35*(8), 1039-1045.
9. Anwar, F.; Latif, S.; Ashraf, M.; Gilani, A.H. *Phytoter. Res.* **2007**, *21*(1), 17-25.
10. Bhuptawat, H.; Folkard, G.K.; Chaudhari, S. J. *Hazard. Mater.* **2007**, *142*(1-2), 477-482.
11. Pollard, S.J.T.; Thompson, F.E.; McConnachie, G.L. *Wat. Res.* **1995**, *29*(1), 337-347.
12. Warhurst, A.M.; McConnachie, G.L., Pollard, S.J.T., *Wat. Res.* **1997**, *31*(4), 759-766.
13. Guo, S.; Peng, J.; Li, W. et al. *Appl. Surf. Sci.* **2009**, *255*, 8443-8449.

14. Fan, M.; Marshall, W.; Daugaard, D.; Brown, R.C. *Bioresour. Technol.* **2004**, *93*, 103-107.
15. Girgis, S.B.; Soliman, M.A.; Nady, A.F. *Micropor. Mesopor. Mat.* **2011**, *142*, 518-525.
16. Jiménez-Cordero, D.; Heras, F.; Alonso-Morales, N.; Gilarranz, M.A.; Rodríguez, J.J. *Chem. Eng. J.* **2013**, *231*, 172-181.
17. Al-Bahri, M.; Calvo, L.; Gilarranz, M.A.; Rodríguez, J.J. *Chem. Eng. J.* **2012**, *203*, 348–356.
18. Rosas, J.M.; Bedia, J.; Rodríguez-Mirasol, J.; Cordero, T. *Ind. Eng. Chem. Res.* **2008**, *47*, 1288-1296.
19. Py, X.; Guillot, A.; Cagnon, B.; Carbon **2003**, *41*, 1533-1543.
20. Heras, F.; Alonso-Morales, N.; Jiménez-Cordero, D.; Gilarranz, M.A.; Rodríguez, J.J. *Ind. Eng. Chem. Res.* **2012**, *51*, 2609-2614.
21. Brunauer, S.; Emmett, E.; Teller, E. *J. Am. Chem. Soc.* **1938**, *60*, 309-319.
22. Barret, E.P.; Joyner, L.G.; Halenda, P.P. *J. Am. Chem. Soc.* **1951**, *73(1)*, 373-380.
23. Gil, A.; Grange, P. *Colloids Surf. A* **1996**, *113*, 39-50.
24. Jagiello, J.; Thommes, M. *Carbon* **2004**, *42*, 1227-1232.
25. Jahirul, M.I.; Rasul, M.G.; Chowdhury, A.A.; Ashwath, N. *Energies* **2012**, *5(12)*, 4952-5001.
26. Jiménez-Cordero, D.; Heras, F.; Alonso-Morales, N.; Gilarranz, M.A.; Rodríguez, J.J. *Biomass Bioenerg.* **2013**, *54*, 123-132.
27. Angin, D. *Bioresource Technol.* **2013**, *128*, 593-597.
28. Katyal, S.; Thambimuthu, K.; Valnix, J. *Renew. Energy.* **2003**, *28*, 713-725.
29. Cordero, T.; Rodríguez-Mirasol, J.; Tancredi, N.; Piriz, J.; Vivo, G.; Rodríguez, J.J. *Ind. Eng. Chem. Res.* **2002**, *41*, 6042–6048.

30. Aksoylu, E.A.; Magdalena, M.; Freitas, M.M.A.; Pereira, M.F.R.; Figueiredo, J.L. Carbon **2001**, *39*, 175–185.
31. Figueiredo, J.L.; Pereira, M.F.R.; Freitas, M.M.A.; Órfão, J.J.M. Carbon **1999**, *37*, 1379-1389.

Table 1. Composition (% w, d.b.) of the carbonized materials obtained under different pyrolysis conditions.

Sample	Elemental composition			
	C	H	N	S
Precursor	50.51	5.77	0.91	0.28
500SH	75.43	3.30	1.29	0.04
600SH	76.73	2.49	1.22	0.03
700SH	79.79	1.78	1.21	0.01
800SH	80.53	1.46	1.25	0.02
500FH	75.53	3.27	1.32	0.03
600FH	77.07	2.72	1.19	0.04
700FH	79.74	2.00	1.21	0.01
800FH	80.55	1.51	1.33	0.02

Table 2. Surface area (m^2g^{-1}) and pore volume (cm^3g^{-1}) of the carbonized materials obtained by pyrolysis.

	S_{DA}	S_{BET}	$V_{\text{micro CO}_2}$	$V_{\text{micro N}_2}$	$V_{\text{meso (2-8 nm)}}$	$V_{\text{mesoTOTAL}}$
500SH	341	66	0.118	0.020	0.007	0.024
600SH	416	310	0.142	0.134	0.004	0.013
700SH	450	139	0.149	0.058	0.004	0.014
800SH	472	8	0.157	0.003	0.000	0.002
500FH	354	26	0.123	0.011	0.001	0.004
600FH	410	224	0.156	0.101	0.003	0.009
700FH	452	7	0.152	0.001	0.001	0.005
800FH	467	3	0.155	0.001	0.000	0.002

Table 3. Specific surface area of chars selected for carbon dioxide adsorption runs

Sample	Starting material	Pyrolysis T (°C)	S _{BET} (cm ³ g ⁻¹)	S _{DA} (cm ³ g ⁻¹)
600FH	Moringa seed husk	600	224	410
800FH	Moringa seed husk	800	3	467
GS800FH	Grape seed	800	54	479

Figure Captions

Figure 1. Selected SEM images of crushed *Moringa oleifera* seed husk.

Figure 2. TGA of Moringa seed husk in N₂ atmosphere at different final temperatures (10°C min⁻¹ heating rate).

Figure 3. TGA experiments (a) isothermal chemisorption tests in air for carbonized material, (b) non-isothermal desorption tests in nitrogen for carbonized material subjected to chemisorption at different temperatures.

Figure 4. Burn-off versus number of activation cycles at different activation conditions.

Figure 5. Specific surface area (BET and DA) versus number of activation cycles under the two different conditions tested.

Figure 6. Variation of S_{BET}/burn-off versus number of cycles at different activation conditions

Figure 7. Micropore volume development from N₂ isotherms along the cycles at the two different activation conditions.

Figure 8. Pore size distribution as obtained by NLDFT method from CO₂ (a) and N₂ (b) isotherms for selected samples: char and activated carbons upon ten cycles at the two different conditions tested.

Figure 9. Selected SEM micrographs of pyrolysed seeds husk (600SH sample).

Figure 10. SEM micrographs of activated samples subjected to desorption at 450°C (a) 180-450C5 and (b) 180-450C10.

Figure 11. SEM micrographs of activated samples subjected to desorption at 900°C (a) 180-900C5 and (b) 180-900C10.

Figure 12. SEM micrograph and micropore size distribution of grape seed char (GS800FH)

Figure 13. Carbon dioxide adsorption kinetic runs for chars prepared from moringa seed husk (MO600FH, MO800FH) and grape seeds (GS800FH).

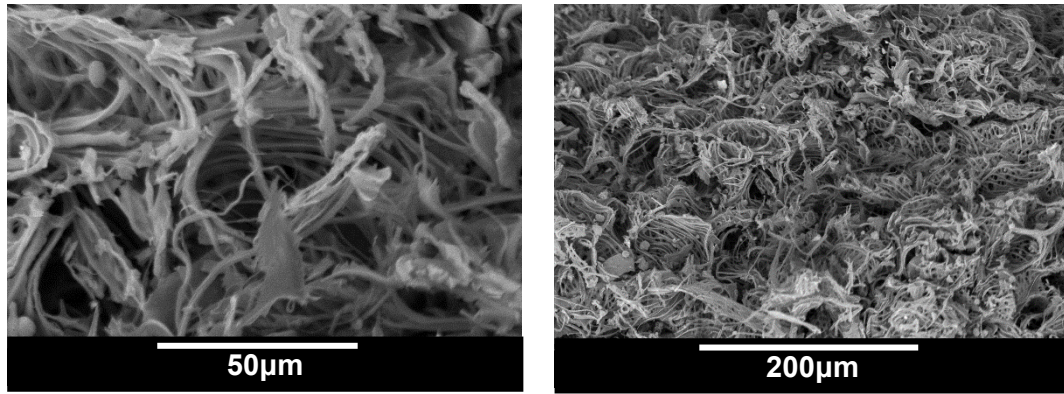


Figure 1. Selected SEM images of crushed *Moringa oleifera* seed husk.

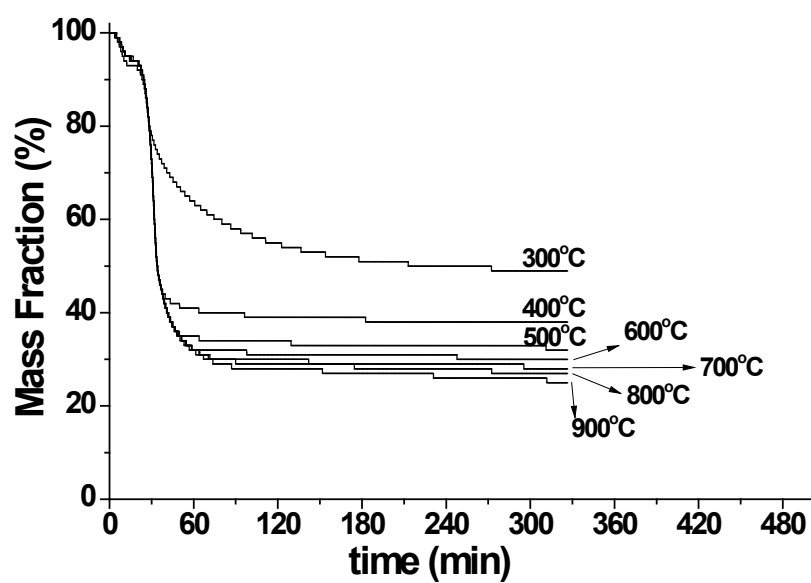


Figure 2. TGA of Moringa seed husk in N₂ atmosphere at different final temperatures (10°C min⁻¹ heating rate).

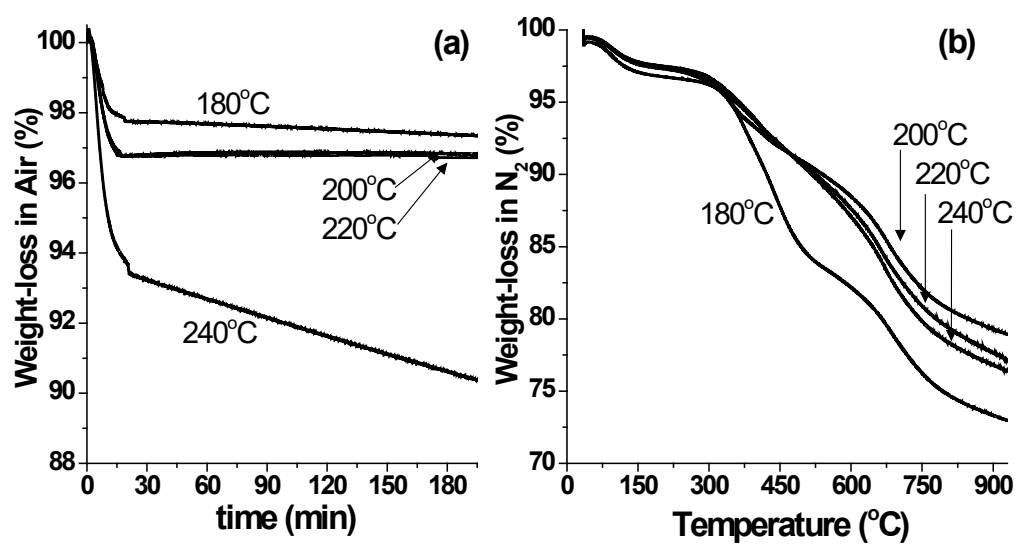


Figure 3. TGA experiments (a) isothermal chemisorption tests in air for carbonized material, (b) non-isothermal desorption tests in nitrogen for carbonized material subjected to chemisorption at different temperatures.

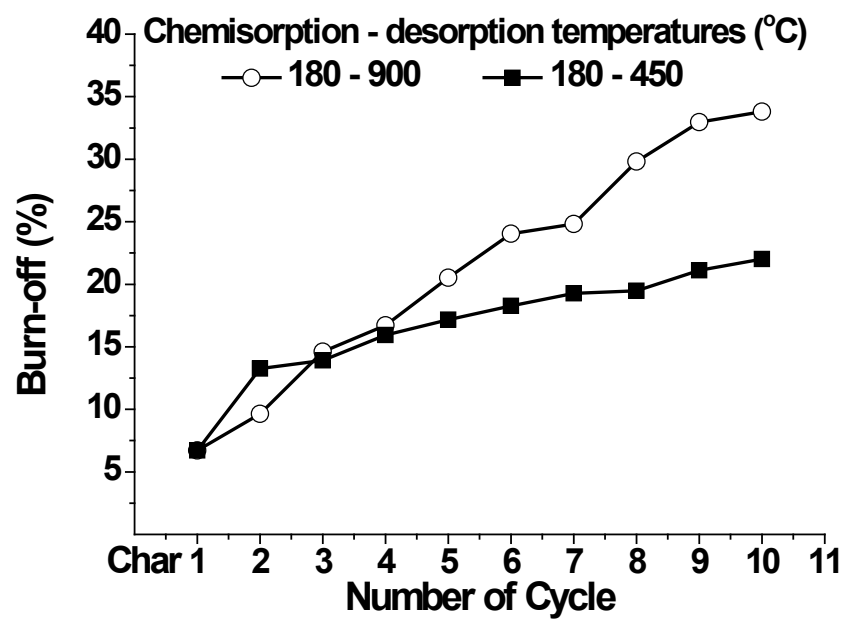


Figure 4. Burn-off versus number of activation cycles at different activation conditions.

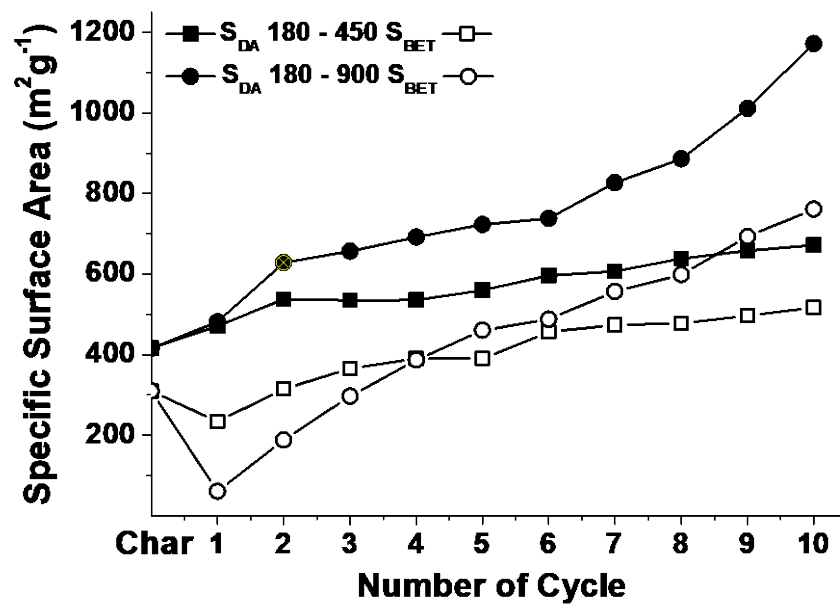


Figure 5. Specific surface area (BET and DA) versus number of activation cycles under the two different conditions tested.

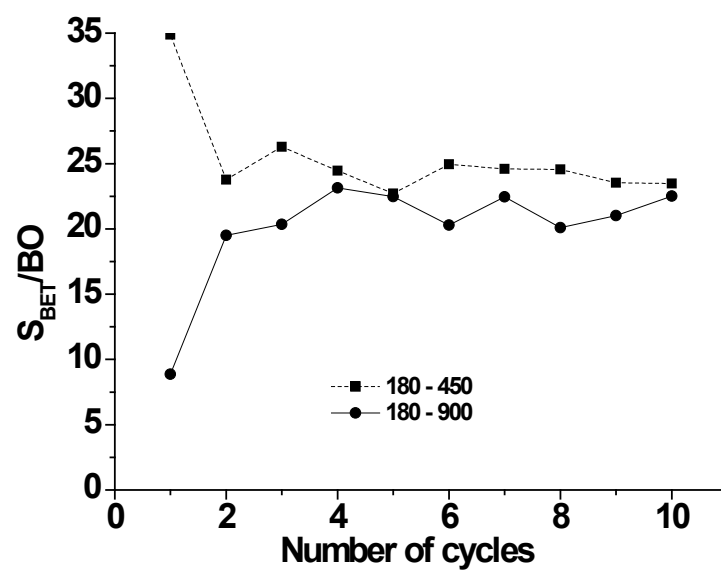


Figure 6. Variation of $S_{\text{BET}}/\text{burn-off}$ versus number of cycles at different activation conditions.

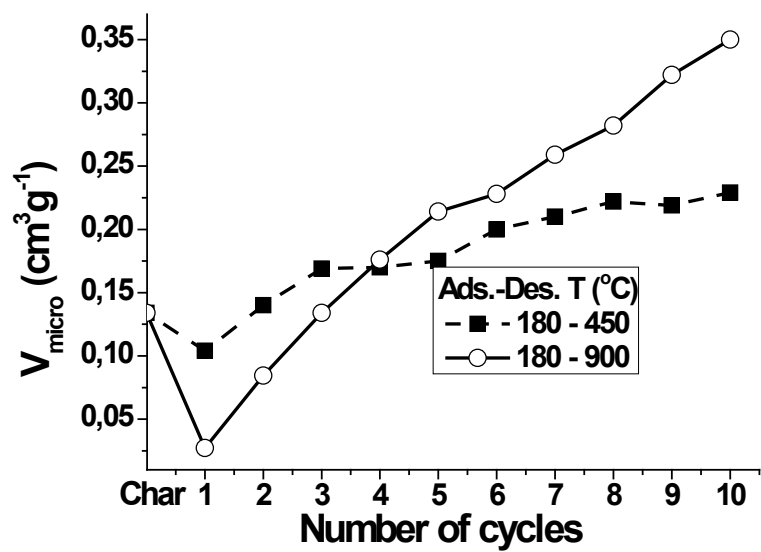


Figure 7. Micropore volume development from N_2 isotherms along the cycles at the two different activation conditions.

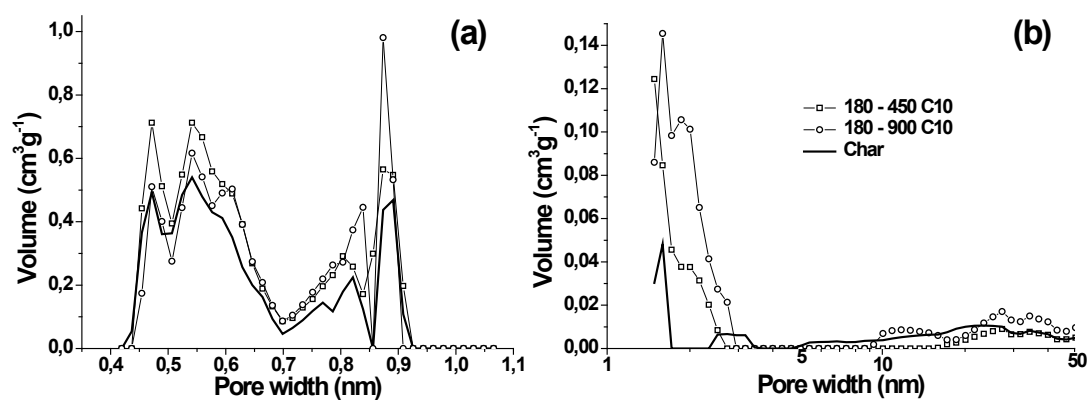


Figure 8. Pore size distribution as obtained by NLDFT method from CO_2 (a) and N_2 (b) isotherms for selected samples: char and activated carbons upon ten cycles at the two different conditions tested.

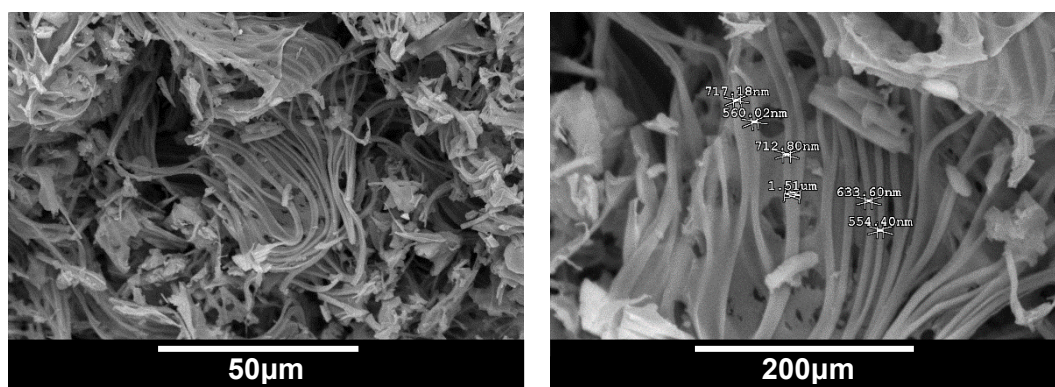


Figure 9. Selected SEM micrographs of pyrolysed seeds husk (600SH sample).

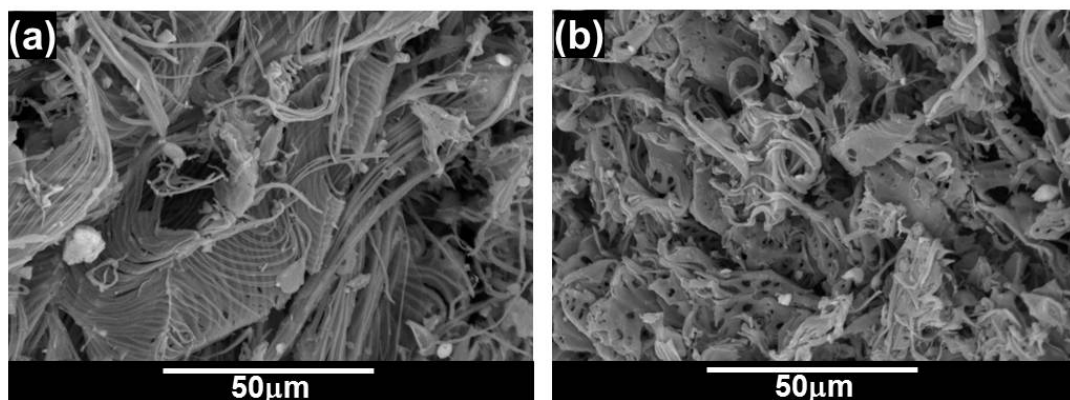


Figure 10. SEM micrographs of activated samples subjected to desorption at 450°C (a) 180-450C5 and (b) 180-450C10.

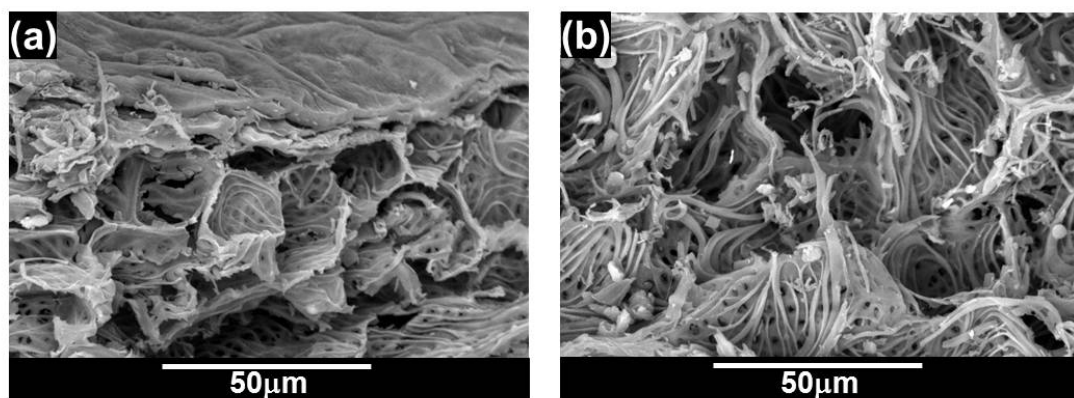


Figure 11. SEM micrographs of activated samples subjected to desorption at 900°C (a) 180-900C5 and (b) 180-900C10.

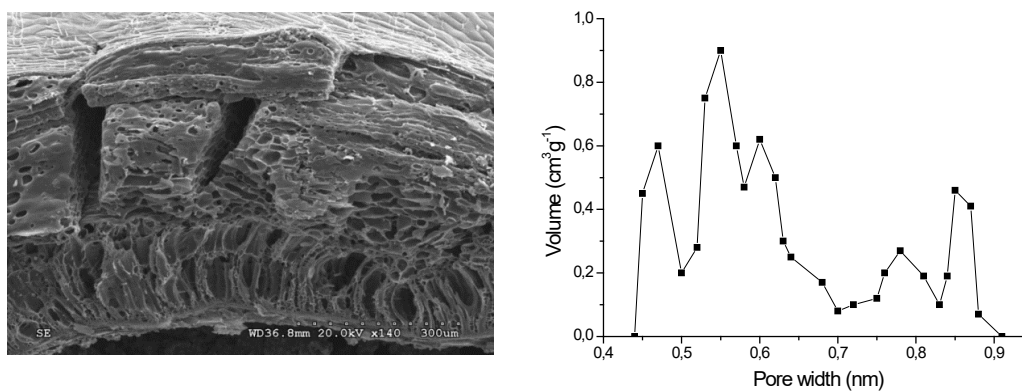


Figure 12. SEM micrograph and micropore size distribution of grape seed char (GS800FH)

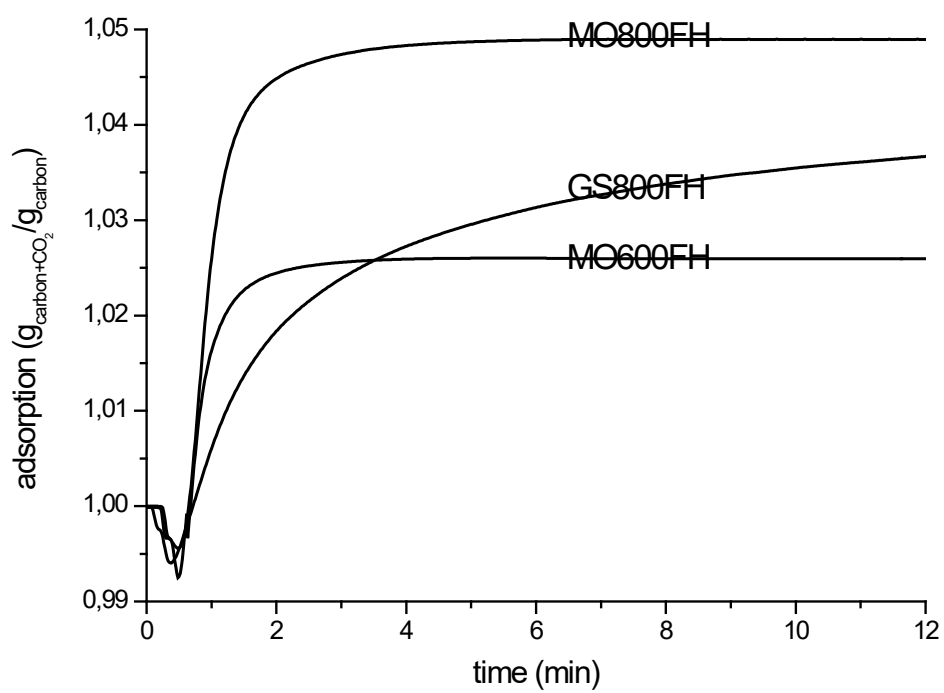


Figure 13. Carbon dioxide adsorption kinetic runs for chars prepared from moringa seed husk (MO600FH, MO800FH) and grape seeds (GS800FH).